# Nanoscale

Accepted Manuscript


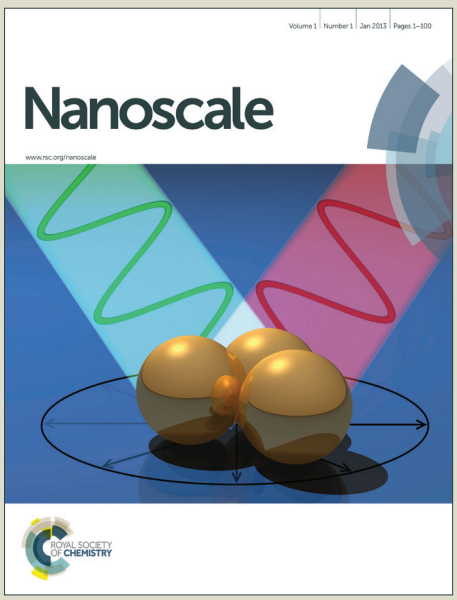





ROYAL SOCIETY OF CHEMISTRY

www.rsc.org/nanoscale

# Detailed Formation Processes of Stable Dislocations in Graphene

Gun-Do Lee [a*], Euijoon Yoon [a], Kuang He [b], Alex W. Robertson [b], Jamie H. Warner [b*]

[a] Department of Materials Science and Engineering, Seoul National University, Seoul 151-742, Republic of Korea

[b] Department of Materials, University of Oxford, Parks Road, Oxford, OX1 3PH, United Kingdom

* Corresponding authors

Email : gdlee@snu.ac.kr , jamie.warner@materials.ox.ac.uk

**Abstract**

We use time-dependent HRTEM to reveal that stable dislocation pairs in graphene are formed from an initial complex multi-vacancy cluster that undergoes multiple bond rotations and adatom incorporation. In the process, it is found that the transformation from the formed complex multi-vacancy cluster can proceed without the increase of vacancy because many atoms and dimers are not only evaporated but also actively adsorbed. In tight-binding molecular dynamics simulation, it is confirmed that adatoms play an important role in the reconstruction of non-hexagonal rings into hexagonal rings. From density functional theory calculation, itIt is also found from simulation that there is a favorable distance between two dislocations pointing away from each other (i.e formed from atom loss). For dislocation pairs pointing away from each other, the hillock-basin structure is more stable than the hillock-hillock structure for dislocation pairs pointing away from each other (i.e formed from atom loss).

## Introduction

Dislocations are important defect structures because they significantly affect the mechanical, chemical and electrical properties of materials[1]. Although the structure of dislocations and their effect on the mechanical and electronic properties of material have been massively studied [2-6], the fundamental formation process of dislocations has been investigated primarily using simulation methods [7-13] and therefore the details are not fully understood due to the prior technical limitations of experiment. Studies that provide a detailed understanding of the formation process of stable dislocations will help make it possible to control dislocations in the future. However, in three dimensional materials, it is very difficult to observe the formation process of dislocations due to the overlap of atoms from the thickness of the sample. The emergence of two dimensional materials such as graphene[14-16] enables the observation of dynamic processes atom by atom without overlap of neighboring atoms which exists in three dimensional materials. High resolution transmission electron microscopy[17, 18] (HRTEM) enables observation of dynamic processes at the atomic level in 2D materials[19-21].

Electron beam irradiation of graphene can generate vacancy defects, Stone-Wales (SW) type bond rotations and also provide kinetic energy to surface adatoms to drive their mobility. The observation of stable dislocations in graphene with a pentagon-heptagon (5-7) pair has been reported[5]. It has been also reported that the dislocation initiates and develops in the reduction of graphene oxide[22]. Dislocation glide and climb by the Stone-Wales (SW) type bond rotation [11, 13] and the evaporation of dimer [12, 13] has also been observed, confirming their mobility within 2D crystals[23]. The formation of dislocation pairs from one-

by-one evaporation of carbon atoms in graphene has been also reported[24]. It has been studied that the addition of dislocations induce the ripple in graphene[25] . In the present study, we focus on the detailed formation process of stable dislocation pairs in graphene originating from large vacancy defect complexes by focused electron beam irradiation and thereafter imaging by HRTEM. The formation process of dislocation pairs are fully analyzed from the formation of multi-vacancy clusters at the atomic scale. Our results help clarify the formation process of dislocations in various other materials.

## Materials and Methods

**Material synthesis** Monolayer graphene was synthesized by atmospheric pressure CVD, with the complete details of synthesis and transfer previously reported in ref. [26] . Graphene was grown on a molten copper sheet (Alfa Aesar, Puratonic 99.999% pure, 0.1 mm thick) of ~1 $cm^2$, resting atop a $cm^2$-sized piece of molybdenum ( Alfa Aesar , 99.95 % pure, 0.1 mm thick). This was loaded into the quartz tube of a CVD furnace, pumped to vacuum and backfilled with argon gas. 100 s.c.c.m. $H_2$/Ar (20% gas mix) and 200 s.c.c.m. pure Ar was flowed, and the furnace was ramped to 1,090°C. Once the temperature was stable the sample was moved into the furnace hot zone and annealed for 30 min. After this the $CH_4$ flow (1% gas mix in Ar) was enabled at 10 s.c.c.m. and the $H_2$/Ar flow reduced from 100 to 80 s.c.c.m., whilst maintaining the pure argon gas line flow at 200 s.c.c.m. This condition was maintained for 90 min to obtain continuous film growth. When completed the $CH_4$ flow was disabled and the sample immediately removed from the furnace hot zone for rapid cooling in the $H_2$ and Ar atmosphere.

A poly (methyl methacrylate) (PMMA) scaffold (8 % wt. in anisole, 495k molecular weight)

was spin cast on to the graphene side of the graphene/copper/molybdenum sample at 4,700 r.p.m. for 60s, and cured at 180°C for 90s. The underlying molybdenum and copper were etched in Fe(III)$Cl_3$ for several days, until just a transparent PMMA/graphene film remained floating on the surface. This was thoroughly cleaned by transferring and floating onto clean deionized water several times, before transfer to a 30% HCl solution for a few minutes. For this step we typically employed a 5-10 minute HCl rinse, but the briefer rinse appeared to help increase the level of intended Fe contamination on the sample when imaged. The sample was rinsed again in DI water for 30 min, and subsequently transferred to a holey silicon nitride TEM grid ( Agar Scientific Y5385). It was then left to dry for about an hour, and then was baked on a hot plate at 150°C for 15 min to remove water and greatly improve sample adhesion.

**Electron microscopy and defect creation** The Oxford - JEOL JEM-2200MCO FEGTEM with CEOS hexapole aberration correctors, operated at an accelerating voltage of 80 kV, was used for electron beam irradiation and imaging. Typical values of residual aberrations after correction are: Defocus: C1 = -239 nm, 2-fold astigmatism: A1=1.054 nm, 3-fold Astigmatism: A2=54.3 nm, Coma: B2=31.52 nm, 3rd order Spherical aberration: C3=-2.106 μm, 4-fold astigmatism: A3=4.119 μm, Star aberration: S3=315.5 nm, 5-fold astigmatism: A4=63.68 μm. See reference [27] for further details. HRTEM images in figures 4 and 5 utilized a maximum filter, as described in reference 19. Defects were created using previously reported method in ref 35 with a beam current density of $1 \times 10^{8}$ $e^{-1}$ $s^{-1}$ $nm^{-2}$ at $2.5 \times 10^{6}$ magnification by focusing the beam to a crossover on a contamination free region of graphene (a small quantity of amorphous carbon in the viewing area is desirable, for on

line correction of low order aberrations).

**Computational Methods** We have performed conjugate gradient minimization method to calculate the formation energy of dislocation by using LAMMPS code [28]. The interatomic forces are described by AIREBO potential [29]. In the simulation, we use a supercell of size ~ 25 x 25 nm containing 23,288 carbon atoms.

We have also carried out DFT total energy calculations. The DFT calculations are performed within the generalized gradient approximation of Perdew-Burke-Ernzerhof (PBE) functional using Vienna *ab initio* simulation package (VASP) code[30]. In the calculation, since the shape of unitcell is distorted by 5-7 pairs, we relax the unit cell with the calculation of stresses. Large enough energy cutoff (800 eV) is chosen to describe correctly stresses and to relax the unitcell. In the simulation, we choose a supercell containing 696 atoms and vacuum region of 30 Å. The structure is relaxed until the force on each atom is smaller than 0.02 eV/Å and the unit cell is also relaxed until the stress is less than 0.1 kbar.

The TBMD simulations are performed using a modified environment-dependent tight-binding (EDTB) carbon potential [31], which was modified from the original EDTB carbon potential [32]. This modified EDTB carbon potential has been successfully applied to investigations of various defect structures in graphene and carbon nanotubes[33-35]. Details of TBMD simulation methods have been described in previous papers[31, 36]. In TBMD simulations, the self-consistent calculations are performed by including a Hubbard-*U* term in TB Hamiltonian to describe correctly charge transfers in carbon atoms of dangling bonds and to prevent unrealistic overestimation of charge transfers[37]. The equations of motions of the atoms are solved by the fifth order predictor-corrector algorithm with a time step of 1.0

fs. All simulations are started at temperature of 3000 K under the canonical control of temperature. The temperature is gradually increased to 5000 K under the linear temperature control to accelerate the dynamics so that structural changes can be observed during the simulation time. Under the electron irradiation in HR-TEM, the creation and transformation of defect structures originate from local overheating by electron irradiation. So, we use high temperature TBMD to approximate the effect of electron beam irradiation on the atomic structure of graphene with good agreement to experimental observations [33, 38, 39]. Even though our simulation temperature is over the melting temperature of graphene, the melting is not observed in a short simulation time scale of ~ nanoseconds because the rate of melting is also dependent on the elapsed time. The velocity scaling method was also used to control the temperature. The unit cell contains 246 carbon atoms. Since during the TBMD simulation the number of atoms in the unit cell will be reduced due to the evaporation of carbon atoms, the unit cell dimensions in the graphene plane are also adjusted accordingly to minimize the stress in unit cell.

## Results and Discussion

We used our previously reported method for defect creation in graphene that utilizes focused electron beam irradiation at 80 kV [40] . In our HRTEM images, we observe that many non-hexagonal defects in damaged graphene reconstruct into a stable dislocation pair with two separate 5-7 pairs. As shown in Figure 1, as time goes by, many non-hexagonal rings are gradually decreased and the stable dislocation pair with two 5-7 pairs is generated. In the initial stage of HRTEM, graphene is damaged by a focused electron beam so that the

defect structures are not identified as shown in Figure S1b. After one minute from Figure S1b, the damaged graphene is reconstructed to form many non-hexagonal rings which can be identified, as shown in Figure 1a and Figure S1c. From Figure 1a, we can confirm that while two dislocations having burgers vector of opposite direction are already formed (Figure S1e), the cores show the unstable structures containing many non-hexagonal rings. After the electron irradiation damages graphene in the initial stage of HR-TEM, it also gives energy to carbon atoms to reconstruct into a more stable structure[40]. This is due to the difference in beam current density between creating defects and imaging defects, which is 4 order of magnitude[20]. When exposed to the focused electron beam (defect creation) many high energy structures are seen to form in a short time-frame, whilst under a lower beam current density (imaging) many of the defect structures slowly relax back to low energy structures, often through the interaction with attached surface adatoms.

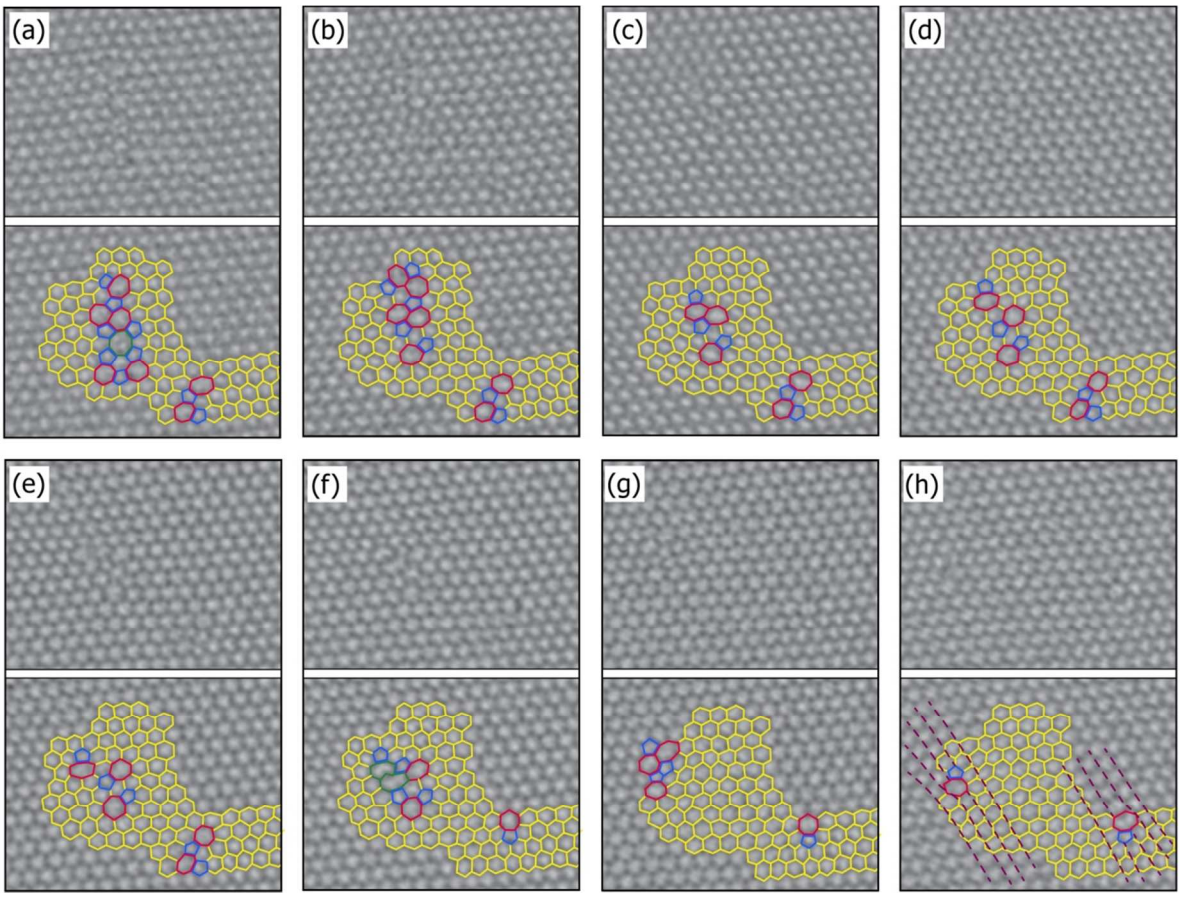


**Figure 1.** Real time dynamics of stable dislocation formation from point defects. Upper and below panel in each figure shows HRTEM image and their structural model, respectively. (a), The image is taken after one minute from focused electron beam, $\Delta t$ = 0 sec. $\Delta t$ is the elapsed time from (a). (b) $\Delta t$ = 20 sec. (c) $\Delta t$ = 47 sec. (d) $\Delta t$ = 121 sec. (e) $\Delta t$ = 195 sec. (f) $\Delta t$ = 225 sec. (g) $\Delta t$ = 268 sec. (h) $\Delta t$ = 362 sec. Yellow and blue colors indicate hexagonal and pentagonal rings, respectively. Red and green colors indicate heptagonal and octagonal rings, respectively. Dashed lines in h show the missing of zigzag lines after 5-7 pairs.

As shown in Figure 1a, after the structure of defective graphene is identified, the formation of many non-hexagonal rings such as pentagons, heptagons and an octagon are observed.

The total number of non-hexagonal rings decreases from Figure 1a to Figure 1c and from Figure 1f to Figure 1h. In the reconstruction process from Figure 1e to Figure 1f, the number of non-hexagonal rings increases with the formation of octagonal rings. It is found that an adatom is adsorbed on the bond of a heptagon to form octagonal rings in Figure 1f and disappears in Figure 1g. The formation of stable dislocation pair is finally observed in Figure 1h. The final structure of the dislocation pair contains eight vacancy units compared with pristine graphene, which is explained in Figure 3.

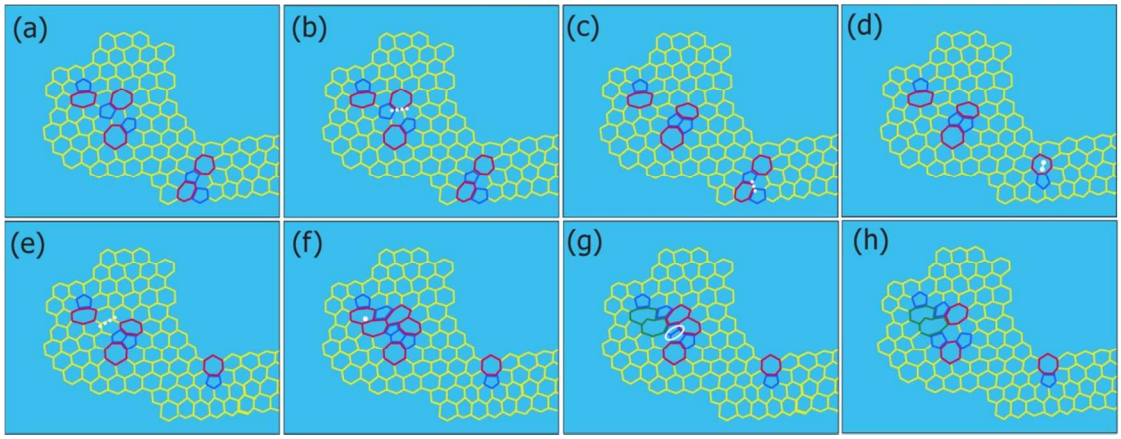


**Figure 2.** Suggested model for possible processes of structural change from Figure 1e to Figure 1f. White dotted lines indicate carbon-carbon bonds undergoing SW type bond rotation at the next step. White dumbbell (in d) and dot (in f) indicate adsorbed dimer and atom, respectively. White ellipse (in g) indicates the evaporated dimer at the next step. We confirm that structural change is very active by SW type bond rotation, the evaporation of dimer, and adsorption of atom and dimer. In f, the increase of non-hexagonal rings is observed with the adsorption of an adatom.

Although HRTEM images from Figure 1e to Figure 1f are taken in 30 seconds, the atomic structure is drastically changed compared to other images in Figure 1. Even though

there a lot of possible routes for the reconstruction process, we suggest one possible route to understand the reconstruction process between the two images, as shown in Figure 2. In the route of reconstruction, all possible processes such as adsorption of adatoms, evaporation of single atoms and dimers, and SW type bond rotation are considered to be relevant. In Figure 2b and 2c, a 5-7 pair coalesces with another 5-7 pair due to the SW type bond rotation. In Figure 2c, another SW type bond rotation reduces the number of non-hexagonal rings. In Fig 2d, the adsorption of a carbon dimer induces the motion of 5-7 pair, the reverse climb compared to the case of the evaporation of a dimer. In Figure 2e, by one more SW type bond rotation, many non-hexagonal rings are generated (Figure 2f). As shown in Figure 2f and Figure 2g, the adsorption of an adatom onto the heptagon forms two octagons and induces the protrusion of a bond. During the HRTEM, it is also found that atoms and dimers diffuse and adsorb to reconstruct the defective graphene. The adsorption of adatoms and dimers is also observed in the analysis of reconstruction process between other two successive HRTEM images (See Figure S2). Those dimers and adatoms are considered to be generated by the electron irradiation of surface residues residing nearby on graphene. It has been reported that the energy barriers for the formation of an adatom (6 - 9 eV) [10, 41] and evaporation of a dimer (10 eV) [12] in non-hexagonal rings of *sp2*-bonded carbon structures are much lower than those (18 - 22 eV)[42, 43] in the pristine graphene. However, in HRTEM, it is very difficult to track the fast diffusion of an adatom due to the small diffusion barrier (0.47 eV) of an adatom[44]. In Figure 2g, the evaporation of a dimer leads to structural model same as the HRTEM image in Figure 1f. The order of the processes suggested in Figure 2 can be reversed in real processes. Nevertheless, the

reconstruction processes such as adsorption of adatom and dimer, evaporation of dimer [12, 13], and SW type bond rotation [11, 13] are inevitable in the formation process of stable dislocation in graphene.

We also suggest the possible processes of reconstruction among the frames of Figure 1 as shown in Figure S2. From the processes, we can count the number of evaporated atoms and adsorbed atoms. It is found that total two carbon atoms are added during the process from Figure 1a to 1h. While carbon atoms are sputtered substantially by the focused electron beam in the very initial stage of HR-TEM, the number of atoms is not much changed after the defect structures are identified even if atoms are evaporated and adsorbed actively. This is compared to another report[24] where the formation of dislocations pointing away from each other was due to the one by one evaporation of carbon atoms. In the present study, it is very important to note that active evaporation and adsorption of atoms occurs during the formation process of stable dislocation pairs. It implies that the reconstruction into the stable dislocation pair can be affected not only by SW type bond rotation but also by evaporated and adsorbed atoms.

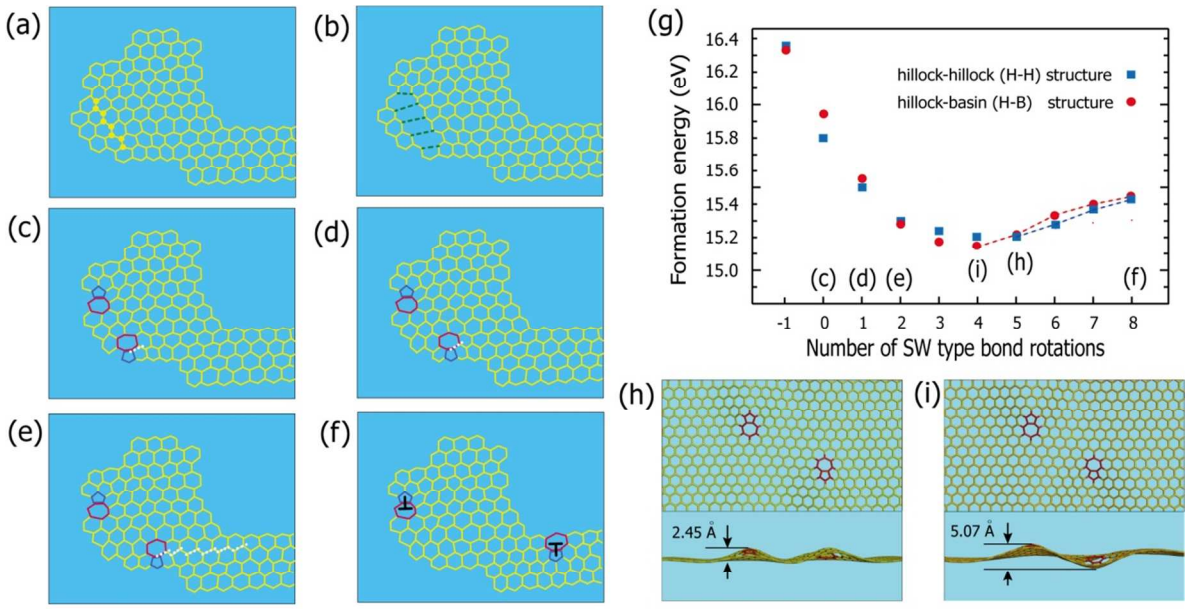


**Figure 3.** (a)-(c) Diagrams showing the formation of dislocation from the missing of eight carbon atoms on zigzag line (a) and the reconstruction (b). (c)-(f) Diagrams showing that the final structure f (Figure 1h) can be formed by successive SW type bond rotations from the dislocation structure c. The structure f can be formed via d and e from the structure c by eight SW type bond rotations indicated by white dotted lines in c, d, and e. (g) The formation energies of dislocation pair with two 5-7 pairs from c to f by employing AIREBO potential. The number '-1' on abscissa indicates the glide of lower 5-7 pair to left-hand side.(h) The DFT structure of the lowest formation energy among hillock-hillock (H-H) structures of dislocation pair. (i) The DFT structure of the lowest formation energy among hillock-basin (H-B) structures of dislocation pair. Top and bottom figures in h and i show top and front views, respectively. Alphabets in g correspond to structures in figure c-f and h-i. Dashed lines in g show the logarithmic increase of formation energy as the distance between the two 5-7 pairs increases from i (or h) to f.

As shown in Figure 3, the dislocation pair generated from eight vacancy units can be simply formed from elimination of eight carbon atoms along the zigzag line (Figure 3a) and its reconstruction (Figure 3b). By the successive Stone-Wales (SW) type bond rotations

(Figure 3c-f), the dislocation become same as the final structure (Figure 1h) from our HRTEM. Figure 3f shows that the formed dislocations point away from each other. Some theoretical reports suggest the formation of dislocation from the linear missing of carbon atoms and the reconstruction[13, 45] as explained in Figure 3a-c. However, our HRTEM shows that the scattered point defects in irradiated graphene can reconstructed into the stable dislocation pair with two separate 5-7 pairs and the process is quite general formation process of stable dislocation in graphene.

We also analyze the structure of the dislocation pair by performing conjugate gradient structural relaxations employing adaptive intermolecular reactive bond order (AIREBO) potential [29]. It has been reported that 5-7 pairs in graphene induce the distortion of two-dimensional plane and form three dimensional hillock structures[46-48]. Stable dislocations formed from reconstruction of vacancies always contain two 5-7 pairs[23, 45]. From two 5-7 pairs, hillock-hillock (H-H) structure could be suggested for the dislocation pair. However, in this study, we suggest the hillock-basin (H-B) structure in which one 5-7 pair is protruded and the other 5-7 pair is recessed. In the calculation, the formation energy of H-B dislocation pair is slightly lower than that of H-H dislocation pair as shown in Figure 2g. In HRTEM images, it is very difficult to discriminate H-H and H-B dislocation pairs because images of HRTEM are taken with two-dimensional projection. Lehtinen et al. [24] reported that in the case of a dislocation pair pointing towards each other (i.e from atom inclusion), a H-H dislocation pair is energetically more favorable than a H-B dislocation pair when two dislocations are close each other. However, in our case of a dislocation pair pointing away from each other, the H-B dislocation pair is energetically more favorable

than the H-H dislocation pair. We also perform the density functional theory (DFT) calculation with smaller unit cell due to the high computational cost to study the structure in detail. While the trend of formation energy from DFT calculation is very similar to that from AIREBO potential, the difference of formation energy is overestimated in the DFT calculation (See Figure S3) compared to AIREBO potential. It is considered to be due to the large stress from smaller unitcell. From DFT calculation, it is found that the height from graphene surface to top of the hillock in a H-H dislocation pair is 2.45 Å and that from the bottom of basin to the top of hillock in a H-B dislocation pair is 5.07 Å. From about 45 degree oriented dipoles in the Figure 3i, we can confirm a general theory of dislocation that the stable dislocation dipoles are formed due to zero shear stress at 45 degree oriented dipoles.[1] We also found that there is an optimum distance between two 5-7 pairs, In the stable dislocation pair reconstructed from eight vacancy units, the optimum distance (distance between centers of heptagons) is 17.7 Å for the H-H structure as shown in Figure 2h and it is 15.4 Å for the H-B structure as shown in Figure 2i. As the distance between two 5-7 pairs increases over the optimum distance, the formation energy increases logarithmically, as shown in Figure 2g. It has been reported [23] that the formation energy is a logarithmic function of distance between two 5-7 pairs without an optimum distance between the dislocation pair formed directly from SW defects without vacancies. Therefore, the optimum distance can be different depending on how many vacancy units are reconstructed into forming the dislocation pair. In the study of dislocations pointing away from each other, the dependence of the optimum distance on the number of vacancy units is an interesting subject of study for the near future.

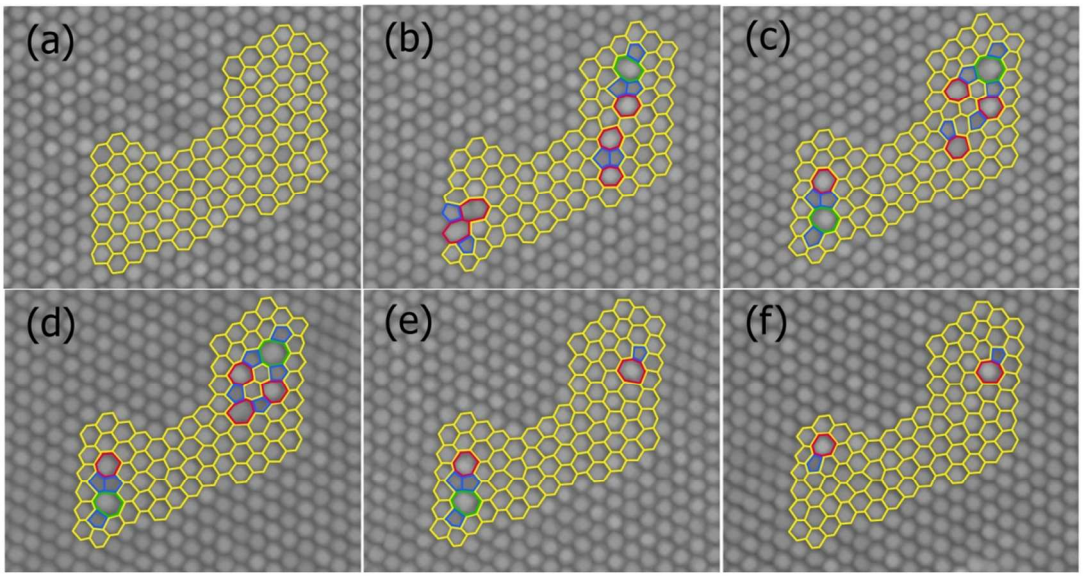


**Figure 4.** The formation of stable dislocation pair from point defects observed in an aberration corrected HR-TEM. Yellow and blue colors indicate hexagonal and pentagonal rings, respectively. Red and green colors indicate heptagonal and octagonal rings, respectively. See figure S4 for original TEM images.

We also find the formation of stable dislocation pair from many defect structures in graphene as shown in Figure 4. The pattern of the formation is very similar to that in Figure 1. Two separate bunches of defects are formed after the focused electron beam irradiation and each bunch is reconstructed into a 5-7 pair as shown in Figure 4f. Carbon atoms are also missing between the two 5-7 pairs and the dislocation pair pointing away from each other is developed. In Figure 4f, comparing with a pristine graphene, we find 18 carbon atoms are missing by the same analysis as Figure 1. This indicates that large number of missing carbon atoms can reconstructed into a stable dislocation pair. The full analysis of the reconstruction process from Figure 4a to 4f is in Figure S4. From the analysis, it is also

confirmed that carbon atoms are actively evaporated and adsorbed. We also reportthe direct formation of a dislocation pair from a divacancy in graphene as shown in Figure 5. Figure 5a shows the combination of divacancy and single vacancy. During the reconstruction process, the divacancy changes the structure while the single vacancy is very stable. The stable single vacancy is considered as a fixed reference for the observation of structural changes of the divacancy. Due to the sequential SW type bond rotation, the two 5-7 pairs are separated and the formation of dislocation pair is observed, shown in Figure 5(f). This dislocation pair formed from the 5-8-5 divacancy is finally transformed back into a stable divacancy structure, 555-777, as shown in Figure 5(g). From DFT calculation, the dislocation pair formed from the SW type bond rotation of divacancy is not stable as shown in Figure 5(h). However, the electron irradiation can give sufficient energy and the expansion or contraction of graphene by defects may give an opportunity to form the dislocation pair.

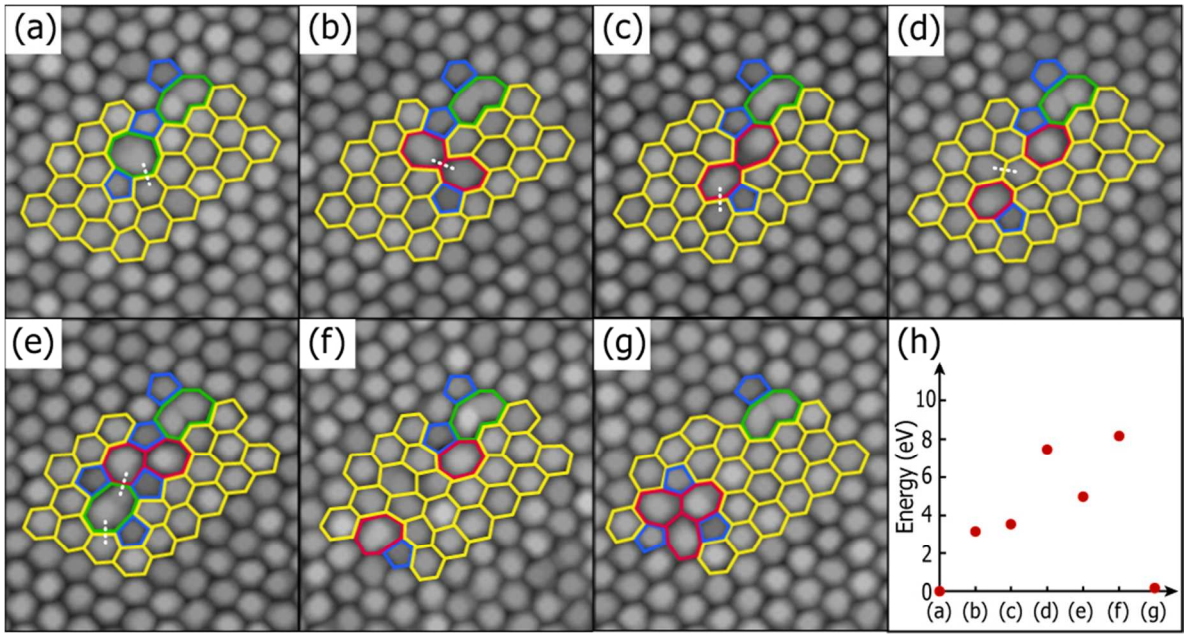

**Figure. 5** (a)-(f) The formation process of dislocation pair from divacancy structure by the separation of 5-7 pair. (g) The final formation of stable divacancy structure. (h) Relative total energy by DFT calculation for each structure. Yellow and blue colors indicate hexagonal and pentagonal rings, respectively. Red colors indicate heptagonal rings. Green colors indicate octagonal or nonagonal rings. White dotted lines indicate the carbon-carbon bond rotating by 90 degree (SW type bond rotation) at next step. See figure S5 for original TEM images.

We also perform tight-binding molecular dynamics (TBMD) simulation to compare with and confirm the TEM observation. Our TBMD simulation method has been successfully applied to study defect structures in graphene[10, 33, 36]. First, we start the TBMD simulation from a reconstructed structure of three vacancy units (Figure 6a). It is confirmed that a vacancy diffuses and coalesces with the defect structure (Figure 6b). In Figure 6c, adatoms are observed to eject from the surface, diffuse on the surface, and evaporate. An adatom is also added in the system to simulate the role of adatom as shown in Figure 6d. It is observed that the adatom coalesces with the collective defects and it gives rise to the temporary increase of non-hexagonal rings as shown in Figure 6e. The temporary increase of non-hexagonal rings due to the coalescence of adatom are in good agreement with the observation from TEM images, as shown in Figure 1f and Figure 2. It is also found that the diffusing adatom helps the transformation of non-hexagonal rings into hexagonal rings. It plays an role of bridging atom which has been reported[38]. This was also observed in previous TBMD simulations [10]. It has been also reported that a diffusing adatom lowers the energy barrier for the SW type bond rotation[49]. In Figure 6g, it is found that the adatom helps the transformation of the SW defect into stable hexagons. Finally, the stable dislocation pair with two 5-7 pairs is formed, as shown in Figure 6h. The TBMD simulation

results are in excellent agreement with HR-TEM images about the formation and evaporation of adatoms, SW type bond rotation, and the formation of the stable dislocation pair with two 5-7 pairs. Although TBMD simulation is performed at very high temperature to observe structural change in short time scale, it is very interesting that the TBMD simulation results are very similar to 80 kV HRTEM results. The TBMD simulation explains the role of adatoms in the structural change of non-hexagonal rings into hexagonal rings. During HRTEM observation, many mobile adatoms are generated by the electron irradiation. Although adatoms give rise to a temporary increase in defects, they play an important role in the reconstruction into the stable dislocation pair.

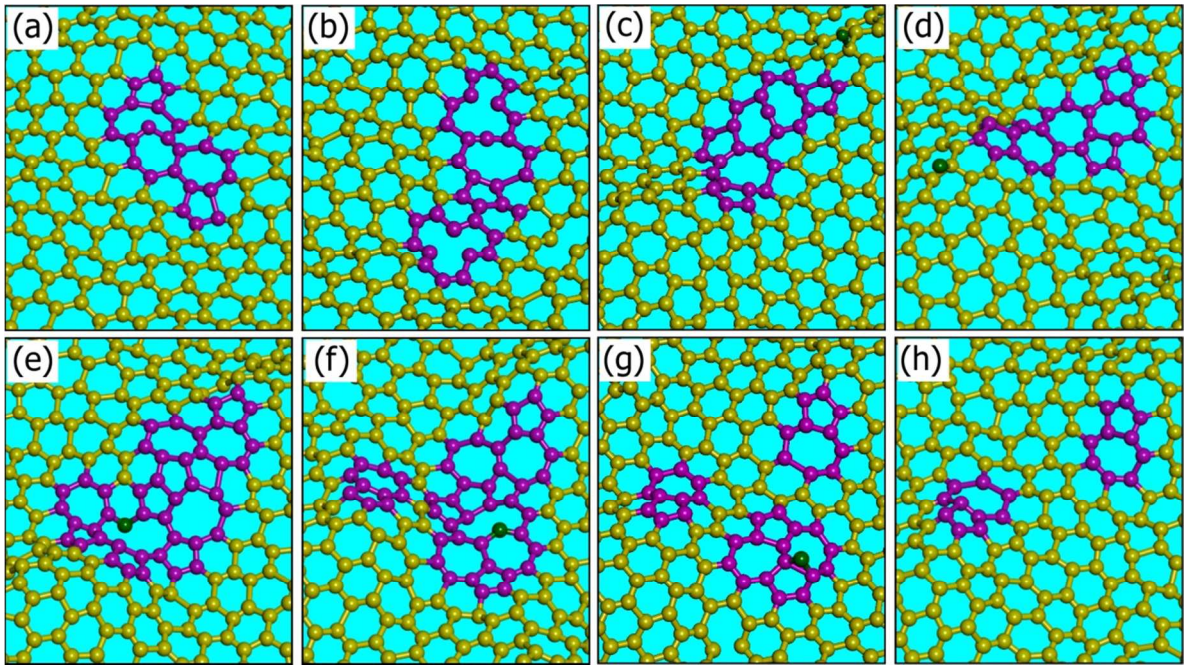


**Figure 6.** Snapshots from the TBMD simulation for dislocation formation process. (a) Temperature ($T$) ~ 4340 K, elapsed time ($t$) = 0.0 ps), (b) $T$ ~ 4860 K, $t$ = 11.3 ps, Single vacancy below diffuses and coalesces with non-hexagonal rings (c) $T$ ~ 5000 K, $t$ = 74.2 ps, Adatom is ejected and evaporated. (d) $T$ ~ 4830 K, $t$ = 85.1 ps, Adatom is added to observe its role for reconstruction of defect structure. (e) $T$ ~ 4760 K, $t$ = 90.6 ps, Non-hexagonal rings are transiently increased with

coalescence of adatom. (f) $T \sim 5130$ K, $t = 93.6$ ps, (g) $T \sim 3620$ K, $t = 163.1.5$ ps, Non-hexagonal rings are reduced with diffusion of an adatom. (h) $T \sim 3690$ K, $t = 167.62$ ps. Stable dislocation pair with two 5-7 pairs is formed. Yellow and violet colors indicate carbon atoms and bonds on hexagonal rings and non-hexagonal rings, respectively. Green colors in c-g indicate adatoms and evaporated carbon atoms.

## Conculsion

We have reported step-by-step details of several pathways leading to stable dislocation pair formation in graphene. In this study, we focus on the detailed formation process of stable dislocation pairs in graphene originating from large vacancy defect complexes. Dislocations observed in irradiated graphene are formed by reconstruction of point defects. Importantly, we reveal that during the HRTEM observations, adatoms and dimers are evaporated and adsorbed actively on graphene surface. The adatoms are active in the reconstruction of non-hexagonal rings. The dislocation pairs formed from a 5-8-5 divacancy were only temporarily stable and reverted back to a divacancy structure. These results provide detailed knowledge regarding the formation of stable dislocation pairs that could be used to help understand the general formation process of dislocation in materials.



## Acknowledgements

GDL thanks the support from the National Research Foundation of Korea (NRF) grant funded by the Korea government (No. 2010-001267, MSIP No. 2013003535) and support from KISTI under the Strategic Supercomputing Applications Support Program (KSC-2013-C3-058). JHW thanks the Royal Society and Balliol College for support.

## Notes and references

[a] Department of Materials Science and Engineering, Seoul National University, Seoul 151-742, Republic of Korea

[b] Department of Materials, University of Oxford, Parks Road, Oxford, OX1 3PH, United Kingdom

Corresponding authors Email : gdlee@snu.ac.kr , jamie.warner@materials.ox.ac.uk

† Electronic Supplementary Information (ESI) available: [HRTEM images of stable dislocation formation (Figure S1). Suggested models for possible reconstruction processes from Figure 1a to Figure 1h (Figure S2). The formation energy of dislocation from DFT calculation (Figure S3). Non-annotated HRTEM images of Figure 4 (Figure S4). Suggested models for possible reconstruction processes from Figure 4a to Figure 4f. (Figure S5). Non-annotated HRTEM images of Figure 5 (Figure S6).]. See DOI: 10.1039/b000000x/

1. J. L. J. P. Hirth, *Theory of Dislocations*, Wiley, New York, 2 edn., 1982.
2. P. Schall, I. Cohen, D. A. Weitz and F. Spaepen, *Science*, 2004, 305, 1944-1948.
3. M. F. Chisholm, S. Kumar and P. Hazzledine, *Science*, 2005, 307, 701-703.
4. S. H. Oh, M. Legros, D. Kiener and G. Dehm, *Nat Mater*, 2009, 8, 95-100.
5. A. Hashimoto, K. Suenaga, A. Gloter, K. Urita and S. Iijima, *Nature*, 2004, 430, 870-873.
6. K. Suenaga, H. Wakabayashi, M. Koshino, Y. Sato, K. Urita and S. Iijima, *Nat Nano*, 2007, 2, 358-360.
7. L. Proville, D. Rodney and M.-C. Marinica, *Nat Mater*, 2012, 11, 845-849.
8. V. Yamakov, D. Wolf, S. R. Phillpot, A. K. Mukherjee and H. Gleiter, *Nat Mater*,

2004, 3, 43-47.
9. C. R. Weinberger, A. T. Jennings, K. Kang and J. R. Greer, *Journal of the Mechanics and Physics of Solids*, 2012, 60, 84-103.
10. G. D. Lee, E. Yoon, N. M. Hwang, C. Z. Wang and K. M. Ho, *Appl Phys Lett*, 2013, 102.
11. B. I. Yakobson, *Appl Phys Lett*, 1998, 72, 918-920.
12. F. Ding, K. Jiao, Y. Lin and B. I. Yakobson, *Nano Lett*, 2007, 7, 681-684.
13. F. Ding, K. Jiao, M. Wu and B. I. Yakobson, *Phys Rev Lett*, 2007, 98, 075503.
14. K. S. Novoselov, A. K. Geim, S. V. Morozov, D. Jiang, Y. Zhang, S. V. Dubonos, I. V. Grigorieva and A. A. Firsov, *Science*, 2004, 306, 666-669.
15. K. S. Novoselov, A. K. Geim, S. V. Morozov, D. Jiang, M. I. Katsnelson, I. V. Grigorieva, S. V. Dubonos and A. A. Firsov, *Nature*, 2005, 438, 197-200.
16. Y. Zhang, Y.-W. Tan, H. L. Stormer and P. Kim, *Nature*, 2005, 438, 201-204.
17. P. E. Batson, N. Dellby and O. L. Krivanek, *Nature*, 2002, 418, 617-620.
18. P. D. Nellist and S. J. Pennycook, *Phys Rev Lett*, 1998, 81, 4156-4159.
19. S. Helveg, C. Lopez-Cartes, J. Sehested, P. L. Hansen, B. S. Clausen, J. R. Rostrup-Nielsen, F. Abild-Pedersen and J. K. Norskov, *Nature*, 2004, 427, 426-429.
20. P. L. Hansen, J. B. Wagner, S. Helveg, J. R. Rostrup-Nielsen, B. S. Clausen and H. Topsøe, *Science*, 2002, 295, 2053-2055.
21. B. Butz, C. Dolle, F. Niekiel, K. Weber, D. Waldmann, H. B. Weber, B. Meyer and E. Spiecker, *Nature*, 2014, 505, 533-537.
22. C. Gomez-Navarro, J. C. Meyer, R. S. Sundaram, A. Chuvilin, S. Kurasch, M. Burghard, K. Kern and U. Kaiser, *Nano Lett*, 2010, 10, 1144-1148.
23. J. H. Warner, E. R. Margine, M. Mukai, A. W. Robertson, F. Giustino and A. I. Kirkland, *Science*, 2012, 337, 209-212.
24. O. Lehtinen, S. Kurasch, A. V. Krasheninnikov and U. Kaiser, *Nat Commun*, 2013, 4, 2098.
25. J. H. Warner, Y. Fan, A. W. Robertson, K. He, E. Yoon and G. D. Lee, *Nano Lett*, 2013, 13, 4937-4944.
26. Y. A. Wu, Y. Fan, S. Speller, G. L. Creeth, J. T. Sadowski, K. He, A. W. Robertson, C. S. Allen and J. H. Warner, *ACS Nano*, 2012, 6, 5010-5017.
27. J. H. Warner, N. P. Young, A. I. Kirkland and G. A. D. Briggs, *Nat Mater*, 2011, 10, 958-962.
28. S. Plimpton, *Journal of Computational Physics*, 1995, 117, 1-19.
29. S. J. Stuart, A. B. Tutein and J. A. Harrison, *The Journal of Chemical Physics*, 2000, 112, 6472-6486.
30. G. Kresse and J. Furthmuller, *Physical Review B*, 1996, 54, 11169-11186.
31. G.-D. Lee, C. Z. Wang, E. Yoon, N.-M. Hwang and K. M. Ho, *Physical Review B*, 2006, 74, 245411.
32. M. S. Tang, C. Z. Wang, C. T. Chan and K. M. Ho, *Physical Review B*, 1996, 53, 979.
33. G.-D. Lee, C. Z. Wang, E. Yoon, N.-M. Hwang, D.-Y. Kim and K. M. Ho, *Phys Rev Lett*, 2005, 95, 205501.
34. G.-D. Lee, C.-Z. Wang, J. Yu, E. Yoon, N.-M. Hwang and K.-M. Ho, *Physical*

*Review B*, 2007, 76, 165413.
35. G. D. Lee, C. Z. Wang, E. Yoon, N. M. Hwang and K. M. Ho, *Appl Phys Lett*, 2010, 97.
36. G.-D. Lee, C. Z. Wang, E. Yoon, N.-M. Hwang and K. M. Ho, *Physical Review B*, 2010, 81, 195419.
37. C. H. Xu, C. Z. Wang, C. T. Chan and K. M. Ho, *Journal of Physics: Condensed Matter*, 1992, 4, 6047.
38. A. W. Robertson, G.-D. Lee, K. He, E. Yoon, A. I. Kirkland and J. H. Warner, *Nano Lett*, 2014, 14, 3972-3980.
39. A. W. Robertson, G.-D. Lee, K. He, E. Yoon, A. I. Kirkland and J. H. Warner, *Nano Lett*, 2014, 14, 1634-1642.
40. A. W. Robertson, C. S. Allen, Y. A. Wu, K. He, J. Olivier, J. Neethling, A. I. Kirkland and J. H. Warner, *Nat Commun*, 2012, 3, 1144.
41. G.-D. Lee, E. Yoon, C.-Z. Wang and K.-M. Ho, *Journal of Physics: Condensed Matter*, 2013, 25, 155301.
42. O. V. Yazyev, I. Tavernelli, U. Rothlisberger and L. Helm, *Physical Review B*, 2007, 75, 115418.
43. A. V. Krasheninnikov, F. Banhart, J. X. Li, A. S. Foster and R. M. Nieminen, *Physical Review B*, 2005, 72, 125428.
44. P. O. Lehtinen, A. S. Foster, A. Ayuela, A. Krasheninnikov, K. Nordlund and R. M. Nieminen, *Phys Rev Lett*, 2003, 91, 017202.
45. B. W. Jeong, J. Ihm and G.-D. Lee, *Physical Review B*, 2008, 78, 165403.
46. O. V. Yazyev and S. G. Louie, *Physical Review B*, 2010, 81, 195420.
47. J. Coraux, A. T. N`Diaye, C. Busse and T. Michely, *Nano Lett*, 2008, 8, 565-570.
48. Y. Liu and B. I. Yakobson, *Nano Lett*, 2010, 10, 2178-2183.
49. I. H. Lee, S. Jun, H. Kim, S. Y. Kim and Y. Lee, *Appl Phys Lett*, 2006, 88.

**TOC graphic**